Desalination and Water Treatment
www.deswater.com
doi: 10.5004/dwt.2022.28748

269 (2022) 141–151
September

Removal of nonylphenol from aqueous solutions using 4-aminoantipyrine grafted Bi_2Te_3/GO with high-performance liquid chromatography with fluorescence detector

Leila Hazratian[a], Nabioallah Mansouri[b], Homayon Ahmad Panahi[c,*], Lobat Taghavi[a], Elham Moniri[d]

[a]*Department of Environmental Science, Faculty of Natural Resources and Environment, Science and Research Branch, Islamic Azad University, Tehran, Iran, emails: L.hazratian@yahoo.com (L. Hazratian), taghavi_lobat@yahoo.com (L. Taghavi)*
[b]*Department of Environmental Engineering, Faculty of Natural Resources and Environment, Science and Research Branch, Islamic Azad University, Tehran, Iran, email: nmansourin@gmail.com*
[c]*Department of Chemistry, Islamic Azad University, Central Tehran Branch, Tehran, Iran, email: h.ahmadpanahi@iauctb.ac.ir*
[d]*Department of Chemistry, Islamic Azad University, Varamin (Pishva) Branch, Iran, email: moniri30003000@yahoo.com*

Received 31 January 2022; Accepted 9 July 2022

ABSTRACT

This novel method, called layer by layer, is composed of alternate layers of graphene oxide and bismuth telluride nanoparticles, and to enhance the adsorption capacity the surface of nanoparticles was modified by 4-aminoantipyrine. A high-performance liquid chromatography with fluorescence detector technique was validated and used for analysis of nonylphenol extracted from environment water samples. Fourier-transform infrared spectroscopy, scanning electron microscopy, energy-dispersive X-ray, thermogravimetric analysis, and X-ray diffraction spectroscopy were applied to characterize the nanoadsorbent. Under the optimum conditions (pH = 5, contact time = 15 min, temperature = 30°C, and initial nonylphenol concentration = 20 mg L^{-1}), the developed technique shown the excellent reusability. Within the 5th cycle, the adsorption potential of recycled nanoadsorbent was restored by nearly 90% and this percentage decreased to 60% in the 8th cycle. The adsorption data fitted well with the Langmuir isotherm model (R^2 = 0.9927) and pseudo-second-order kinetic model (R^2 = 1). The obtained nanoadsorbent possess the highest sorption capacity (43.47 mg g^{-1}). Recoveries, at 1 μg mL^{-1} concentration level, ranged from 89% to 98% with relative standard deviations lower than 5% (n = 3). The results of nonylphenol removal from the environment samples shown the great applicability of nanoadsorbent for the removal of nonylphenol.

Keywords: Nonylphenol; Bismuth telluride; Removal; 4-aminoantipyrine; Layer by layer; Graphene oxide

1. Introduction

Nonylphenol (NP), as one of the most important industrial raw material, have been used for different commercial products such as paints and latex paints, textiles, plastics, washing agents, adhesives, paper, petroleum recovery chemicals, etc. Also, NP is used in lubricating oil additives and manufacturing antioxidants [1,2]. The disadvantages of NP are an estrogenic activity, low degradation rates and high hydrophobicity [3]. NP is well known as micro pollutants having a potential hazard to the human health, animal and environment. Thus, it is important to develop method for the detection NP in environmental samples. It is important to develop an accurate and ultrasensitive procedure for the detection of NP residue in aqueous

* Corresponding author.

environment. NP is hazardous pollutants commonly found in aqueous solutions.

Their removal is a high selectivity for avoiding adverse effects on the environment [4]. To date, researchers have driven extensive research efforts concerning the removal of NP from water samples using nanoadsorbents. Zhou et al. [5] prepared magnetic nanoparticle as a nanoadsorbent for the removal of NP. Haciosmanoglu et al. [6] prepared a nano zero-valent iron nanoparticles and used it for the removal of NP from an aqueous solution. Therefore, a variety of analytical techniques based on high-performance liquid chromatography (HPLC) [7,8], gas chromatography coupled with mass spectroscopy (GC-MS) [9], liquid chromatography-tandem mass spectrometry (LC-MS/MS) [10,11] have been developed for identification of NP.

Also, numerous methods such as adsorption [12–14], membrane separation [15], catalytic oxidation [16], and biological method [17] have been applied to remove NP. Adsorption technology has a great potential in treating varieties of pollutants, due to its low cost and high removal efficiency [18].

Graphene oxide (GO) has a large surface area, thermal stability, adsorption capacity in the nanoscale, optical transmission, high electrical conductivity and good mechanical. GO is an effective adsorbent in removing pollutant from the aqueous solution [19]. Owing to the abundant oxygen-containing groups such as hydroxyl, epoxy and carboxyl, GO is facile for functionalization by non-covalent or covalent bonding interactions in removing contaminations from water samples [20]. Functionalization of GO is an effective process for the removal of some of the problems associated with using GO as a sorbent. Therefore, researchers have reported functionalized GO as the sorbent for the sorption of organic pollutants and heavy metals [21].

Bismuth telluride (Bi_2Te_3) as one of the most excellent thermoelectric materials, has high thermoelectric properties and low thermal conductivity [22]. Liang et al. [23] developed Bi_2Te_3/graphene bulk materials by a hydrothermal method. Agarwal et al. [24] developed Bi_2Te_3/graphene bulk materials by a cold pressing method. Also, Kumar et al. [25] prepared Bi_2Te_3/reduced GO nanocomposites by a refluxing process.

Layer-by-layer self-assembly is considered as a relatively facile process which could consecutively deposit single molecular layers onto planar substrate and to form tunable multilayers of organic molecules at least in one dimension. Besides, layer-by-layer assembly can be applied to spherical particles, inside pores, planar surfaces, and surfaces with more complex geometries [26]. For example, Jiang et al. [27], developed facile synthesis of layer-by-layer decorated GO based magnetic nanocomposites for β-agonists/dyes adsorption removal and bacterial inactivation in wastewater. To-date, there are no reports on GO based layer-by-layer with Bi_2Te_3.

In the present work, the main objective of this work was to synthetize a facile layer-by-layer GO with Bi_2Te_3 nanoparticles as a nanoadsorbent for NP removal from water and industrial wastewater samples for the first time. Certain analytical factors on the removal of NP such as pH, contact time, temperature, and initial NP concentration effects were studied. The resulting Bi_2Te_3/GO@4-AA nanocomposites have the major advantages for high capacity, which were characterized by different techniques. The adsorption isotherms, kinetics, and reusability of Bi_2Te_3/GO@4-AA were tested to explain the adsorption behavior of nanoparticles. These results suggest the potential utilization of Bi_2Te_3/GO@4-AA for the removal of NP from environment water samples.

2. Experimental

2.1. Materials

Standard solution of NP (CAS: 84852-15-3) was purchased from Sigma-Aldrich (Steinheim, Germany) which was analytic grade reagents without any further purification. Tellurium dioxide (TeO_2, purity > 97%), sodium tartrate ($C_4H_4Na_2O_6$, purity > 98%), bismuth(III) nitrate pentahydrate ($Bi(NO_3)_3{\cdot}5H_2O$, purity > 98%)), potassium borohydride (KBH_4, purity > 98%), potassium hydroxide (KOH), 4-AA (purity > 99%), sodium metaperiodate ($NaIO_4$, purity > 99%) were obtained from Merck Company (Darmstadt, Germany). GO (Multilayer, www.nanoshel.com, USA, United States) was supplied from nanoshel. All other reagents, including methanol (MeOH), ethanol (EtOH), acetone (ACE), and hydrochloric acid (HCl) were of HPLC grade and obtained from Sigma-Aldrich Chemical Company. The stock and internal solutions of NP at concentrations of 100 mg L^{-1} were prepared in deionized (DI) water and kept in the dark at 4°C. Ultrapure water (18.2 MΩ) was obtained from a Milli-Q water ion-exchange system (Millipore, Bedford, MA, USA), and was used in all the experimental work.

2.2. Instrumentations

The shape and surface morphology of the as-prepared samples were observed by scanning electron microscopy equipped with an energy-dispersive X-ray spectrometer (SEM/EDX, MIRA3, TE-SCAN, Czech Republic). The Fourier transform infrared spectrophotometer (FT-IR, NEXUS 870, American Thermo Nicolet Company) was used to measurement of functional groups. The thermal characteristics of the nanoparticles were determined by using a thermogravimetric analyzer (TGA, SETARAM Inc., Franc) in the air atmosphere (10°C min^{-1}). The crystal structure of nanoparticles were recorded by X-ray diffraction (XRD, Seifert 3003TT, Berlin). The UV-Vis scanning spectrophotometer (UV- DR6000, HACH, Germany) was used for determining NP concentration onto nanoadsorbent in aqueous solution. The chromatographic separations were carried out by a high-performance liquid chromatography (HPLC; Alignment Cary 100), column (C_{18} column, 4.6 × 150 mm, Wilmington, DE, USA), fluorescence detector (λ_{ex}: 222 nm, λ_{em}: 305 nm). Analyte separations were carried out by mobile phase consisting of water-methanol (10:90, v/v), injection volume of 20 μL, detection wavelength at 280 nm, and flow rate at 2 mL min^{-1}.

2.3. Synthesis of Bi_2Te_3/GO@4-AA

2.3.1. layer-by-layer of the GO with Bi_2Te_3

Layer-by-layer of GO with Bi_2Te_3 was synthesized as follows: Briefly: 1 g of GO was dispersed into 80 mL DI water

by ultra-sonication (KQ-100DE ultrasonic, Jiangsu, China) for 1 h. The mixture of 2 g sodium tartrate, 0.48 g TeO_2, and 4.5 g KOH was added into the above solution. The obtained solution was shaken for 30 min. This solution was mixed with 0.97 g of Bi $(NO_3)_3 \cdot 5H_2O$. After 2 h stirring reaction, 1.2 g of KBH_4 was added to the solution, and the mixture was stirred for 30 min at 25°C. The solution was transferred to teflon-lined stainless steel autoclave, then the autoclave was capped and heated for 24 h at 180°C to get the Bi_2Te_3/GO composite. Finally, the precipitated product was washed by using double DI water and ethanol.

2.3.2. Synthesis of the 4-AA-modified Bi_2Te_3/GO

At first, 4.28 g of $NaIO_4$ was dissolved in 100 mL of DI water. Next, 3 g of Bi_2Te_3/GO was added into the above solution. This mixture was kept stirring for 4 h at 25°C. The obtained precipitate was washed with DI water to remove unreacted reagents and then dried in a vacuum for 24 h. Subsequently, 0.5 g of 4-AA and 3 g of Bi_2Te_3/GO were added to the 150 mL of ethanol solution under vigorous stirring. Under nitrogen protection, the above solution was agitated at 25°C for 7 h. After the reaction, product was collected and washed three times with double DI water: acetone (9:1, v/v) solution. The schematic representation of preparation of Bi_2Te_3/GO@4-AA is shown in Fig. 1.

2.4. Batch adsorption experiments

All batch adsorption tests were carried out in a micro-tubes at room temperature (25°C) on a thermostat shaker with a shaking speed of 250 rpm. NP solution at initial concentration (20 mg L^{-1}) were prepared by diluting the mixed stock standard solution with DI water. 0.01 g Bi_2Te_3/GO@4-AA was added to 25 mL of the above solution. The initial pH was adjusted to 5 using Magic buffer (1.43 mL of CH_3COOH (0.05 M), 1.67 mL of H_3PO_4 (0.06 M), 1.2 g of H_3BO_3 (0.04 M), and NaOH (2 M)). Agitation of these micro-tubes was conducted for 15 min. After that, the precipitate was centrifuged (EBA20, Tuttlingen, Germany) at 5,000 rpm for 10 min. Finally, the concentration of NP in supernatant was determined by using UV-Vis spectrophotometry. The removal efficiency of Bi_2Te_3/GO@4-AA for NP was calculated by using the following equation:

$$\%R = 100 \times \frac{\left(C_0 - C_e\right)}{C_0} \tag{1}$$

where R represents the removal efficiency of Bi_2Te_3/GO@4-AA for NP. C_0 (mg L^{-1}) and C_e (mg L^{-1}) denote the initial and equilibrium concentration of NP, respectively.

2.5. Adsorption isotherm studies

To study the isotherm experiments, 0.01 g of Bi_2Te_3/GO@4-AA was added to 25 mL solutions with different concentrations (2–40 mg L^{-1}) in micro-tubes, and shaken using a rotary shaker. After 45 min, the samples were centrifuged at 5,000 rpm for 10 min, and finally the concentration of the NP was measured by using a UV-Vis spectrophotometry (λ_{max} = 280 nm). The Langmuir [28], Freundlich [29], Temkin [30] and Dubinin–Radushkevich [31] models

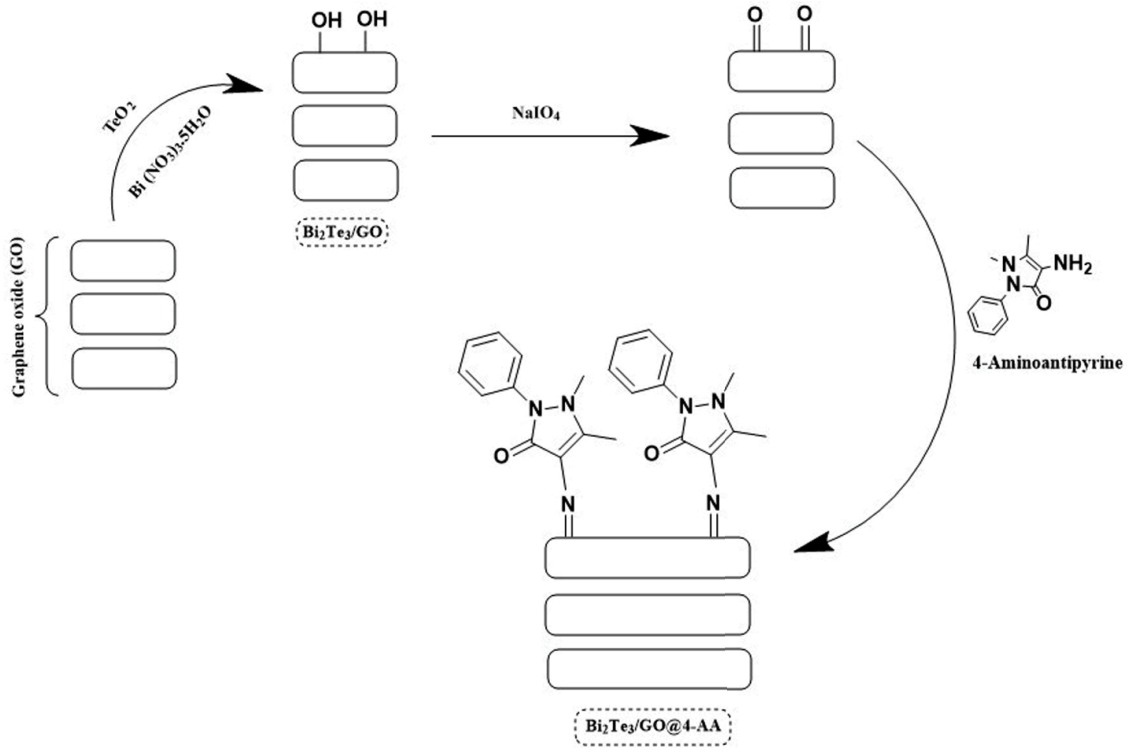

Fig. 1. Schematic illustration synthesis of Bi_2Te_3/GO@4-AA.

were employed to investigate the adsorption isotherms. The linear form of the isotherm model equations can be represented as follows:

$$\text{Langmuir isotherm equation: } \frac{C_e}{q_e} = \frac{1}{K_L q_{\max}} + \frac{C_e}{q_{\max}} \quad (2)$$

$$\text{Freundlich isotherm equation: } \ln q_e = \frac{1}{n \ln C_e} + \ln K_f \quad (3)$$

$$\text{Temkin isotherm equation: } q_e = \frac{RT}{b \ln C_e} + \frac{RT}{b \ln A} \quad (4)$$

$$D-\text{R isotherm equation: } \text{Ln} q_e = \ln q_s - k_{\text{DR}} \varepsilon^2 \quad (5)$$

where C_e (mg L^{-1}), q_e (mg g^{-1}), $q_{\max}$ (mg g^{-1}) denote the NP concentration at equilibrium, the equilibrium sorption capacity, the maximum adsorption capacity, respectively. K_L (L mg^{-1}), K_f (mg g^{-1})(L $mg^{-1})^{1/n}$, and K_{DR} (mol^2 kJ^{-2}) represent the Langmuir, Freundlich, and Dubinin–Radushkevich isotherm constant, respectively. In the Temkin isotherm equation, b (J mol^{-1}; $B = RT/b$) represents the constant related to the heat of NP sorption, R (8.314 J mol^{-1} K^{-1}) represents the universal gas constant, and T (K) represents the temperature. Also, A (L g^{-1}) is the Temkin constant. In the Dubinin–Radushkevich isotherm equation, ε (kJ mol^{-1}) is the Polanyi potential.

2.6. Adsorption kinetic studies

To investigate the kinetic experiments, 0.01 g of nanoadsorbent was added to 25 mL solutions at concentration (20 mg L^{-1}) in micro-tubes and shaken using a rotary shaker. The experiments were performed at different time intervals. After that, the solutions were centrifuged at 5000 rpm for 10 min, and finally the concentration of the NP was measured by using a UV-Vis spectrophotometry ($\lambda_{\max}$ = 280 nm). The pseudo-first-order (PFO), pseudo-second-order (PSO), and intraparticle diffusion (IPD) [32–34] models were employed to study the adsorption kinetics. The linear form of the kinetic model equations can be expressed as follows:

$$\text{PFO kinetic equation: } \log\left(q_e - q_t\right) = \log q_e - \frac{k_1 t}{2.303} \quad (6)$$

$$\text{PSO kinetic equation: } \frac{t}{q_t} = \frac{1}{k_2 q_e^2} + \frac{t}{q_e} \quad (7)$$

$$\text{IPD kinetic equation: } q_t = k_p t^{1/2} + C_i \quad (8)$$

where q_e and q_t represent the adsorption amount of NP at equilibrium and at time, respectively (mg g^{-1}). k_1 (min^{-1}), k_2 (g mg^{-1} min^{-1}), and k_p (g mg^{-1} $min^{-0.5}$) represent the PFO, PSO and IPD rate constant, respectively. Also, C_i (mg g^{-1}) represents the intercept.

2.7. Determination of NP in environment water samples

River water samples were collected from the Kan River (Tehran, Iran). Also, well water samples were collected from Tehran, Iran. Industrial wastewater samples were obtained from dying wastewater treatment plants (Karaj, Iran). All samples were kept in glass bottles in darkness and filtered through a 0.45 membrane before use. At first, 0.01 g of the Bi_2Te_3/GO@4-AA was added into 7 mL of NP solution (1 mg L^{-1}) at pH 5, and agitated for 10 min. Then, the supernatant was collected by centrifugation. Next, the sample was eluted with mobile phase (methanol: water; 90:10) by stirring for 5 min. The precipitate was centrifuged and the supernatant of NP in water/methanol was determined by HPLC technique.

3. Results and discussion

3.1. Characterization of Bi_2Te_3/GO@4-AA

The Fourier-transform infrared spectroscopy (FTIR) spectra of GO, Bi_2Te_3/GO, and Bi_2Te_3/GO@4-AA are shown in Fig. 2a. For Go, Absorptions at 1,625; 1,387 and 1,061 cm^{-1} were related to the C=C bond (resulting from skeletal vibrations of un-oxidized graphite domains), C–OH stretching bond, and C–O stretching peak respectively, indicating that the graphite sheets were oxidized to form GO sheets. The characteristic absorption peak at 3,429 cm^{-1} can be related to –OH stretching vibration. Moreover, in comparison with GO, the FTIR spectra of Bi_2Te_3/GO presented characteristic peaks at 2,829 and 1,383 cm^{-1}, which related to the adsorption peaks of the aliphatic C–H stretching and CH_2 vibrations, respectively. The increase in the adsorption intensity of the above peaks of GO to Bi_2Te_3/GO shows that the Bi_2Te_3 nanoparticles were successfully fabricated at GO sheets. For Bi_2Te_3/GO@4-AA, the presence of the characteristic adsorption peak at 1,564 cm^{-1} correspond to the C–N (amine groups) indicated the successful modification of 4-AA to the Bi_2Te_3/GO.

XRD patterns were investigated to identify the crystalline structure of GO, Bi_2Te_3/GO and Bi_2Te_3/GO@4-AA (Fig. 2b). The sharp and broad peak in GO at 2θ = 11° can related to the creation of the oxygen-containing functional groups on the surfaces of GO. Fig. 2b indicates the XRD patterns of Bi_2Te_3/GO and Bi_2Te_3/GO@4-AA. As shown are XRD patterns, diffraction peaks at 2θ = 28°, 38° and 41° are confirmed by the presence of Bi_2Te_3 nanoparticles and modified of amine groups on Bi_2Te_3/GO surfaces. The adsorption intensity of the peaks decreased slightly after grafting of amine groups. This confirms that the grafting of 4-AA did not change the crystal structure.

Fig. 2c indicates the TGA curves of GO, Bi_2Te_3/GO, and Bi_2Te_3/GO@4-AA. As can be seen from Fig. 2c, GO remained about 5% residues after heated to 1,000°C under air atmosphere. The weight loss below 150°C was attributed to the evaporation of adsorbed water. The mass loss (45%) observed between 400°C and 600°C was related to the degradation of GO skeleton. For Bi_2Te_3/GO, it began to decompose at about 230°C due to the decomposition of organic compounds on GO surface. For Bi_2Te_3/GO@4-AA, the first weight loss occurred at 450°C; this can be related to the decomposition of the Bi_2Te_3/4-AA groups on the GO surface. The remaining

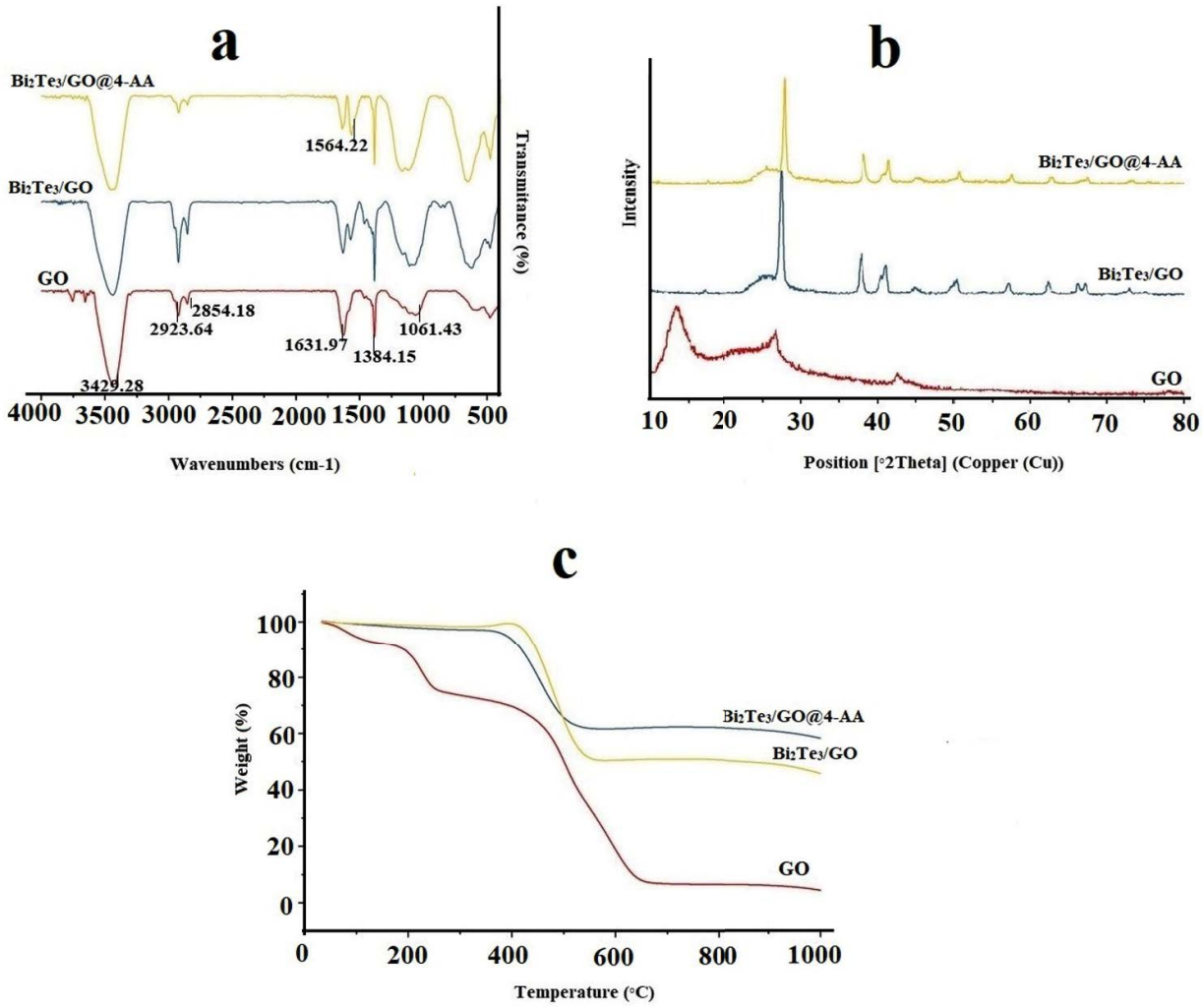

Fig. 2. (a) FTIR spectra, (b) XRD patterns and (c) thermograms of GO, Bi_2Te_3/GO and Bi_2Te_3/GO@4-AA.

weight loss was related to the degradation of GO skeleton. Also, Bi_2Te_3/GO@4-AA only remained 53.18% residues.

The field-emission scanning electron microscopy (FE-SEM) images of GO, Bi_2Te_3/GO and Bi_2Te_3/GO@4-AA together with their respective EDX spectrum are shown in Figs. 3 and 4, respectively. As can be seen in Fig. 3a, the morphology of GO has a typical wrinkled sheet-like structure with the smooth surface. As shown in Fig. 3b, bulk particles of Bi_2Te_3 are well decorated onto the GO nanosheets with an average size of 25 nm. According to Fig. 3c, it reveals that the Bi_2Te_3/GO@4-AA particles have a spherical shape and highly mono dispersed with a relatively uniform size. The EDX spectrum of Bi_2Te_3/GO and Bi_2Te_3/GO@4-AA shown that the elements of carbon, oxygen, bismuth, tellurium, potassium, sodium and boron were in Bi_2Te_3/GO and Bi_2Te_3/GO@4-AA (Fig. 4). The elements ratio of carbon, oxygen, bismuth, tellurium, potassium, sodium and boron is 53.88%, 10.13%, 15.94%, 13.54%, 3.59%, 0.27%, and 2.64% in Bi_2Te_3/GO, respectively. Otherwise, the respective ratios of these elements in Bi_2Te_3/GO@4-AA are 54.70%, 9.36%, 10.09%, 5.92%, 0.47%, 0.19%, and 2.84%. Also, nitrogen element was evenly distributed on the surface of Bi_2Te_3/GO, showing the presence of 4-AA. Then, due to the presence of nitrogen element on the Bi_2Te_3/GO, the percentage of bismuth and tellurium was decreased.

3.2. Optimization studies

3.2.1. Influence of pH, pH_{PZC}, contact time, initial concentration, and temperature on the removal efficiency

The solution's pH is one of the important parameters on the removal efficiency, because it affect the structure of nanoadsorbate and surface charges of nanoadsorbent. The pH of the solution was measured between at the pH range of 3 and 9 using magic buffer. The obtained results indicated the removal efficiency of NP was increased from 60% to 91% at a range of pH 3 to pH 5. On the other hand, the removal efficiency of NP decreased dramatically as the pH was increased from 5 to 9. Accordingly, the optimum pH value for NP was 5 (Fig. 5a). To agreement the precision of evaluating optimum pH, the point of zero charge (pH_{PZC}) was considered. The PZC of the Bi_2Te_3/GO@4-AA that contains a negative charge at pH amounts of less than 5.4, but

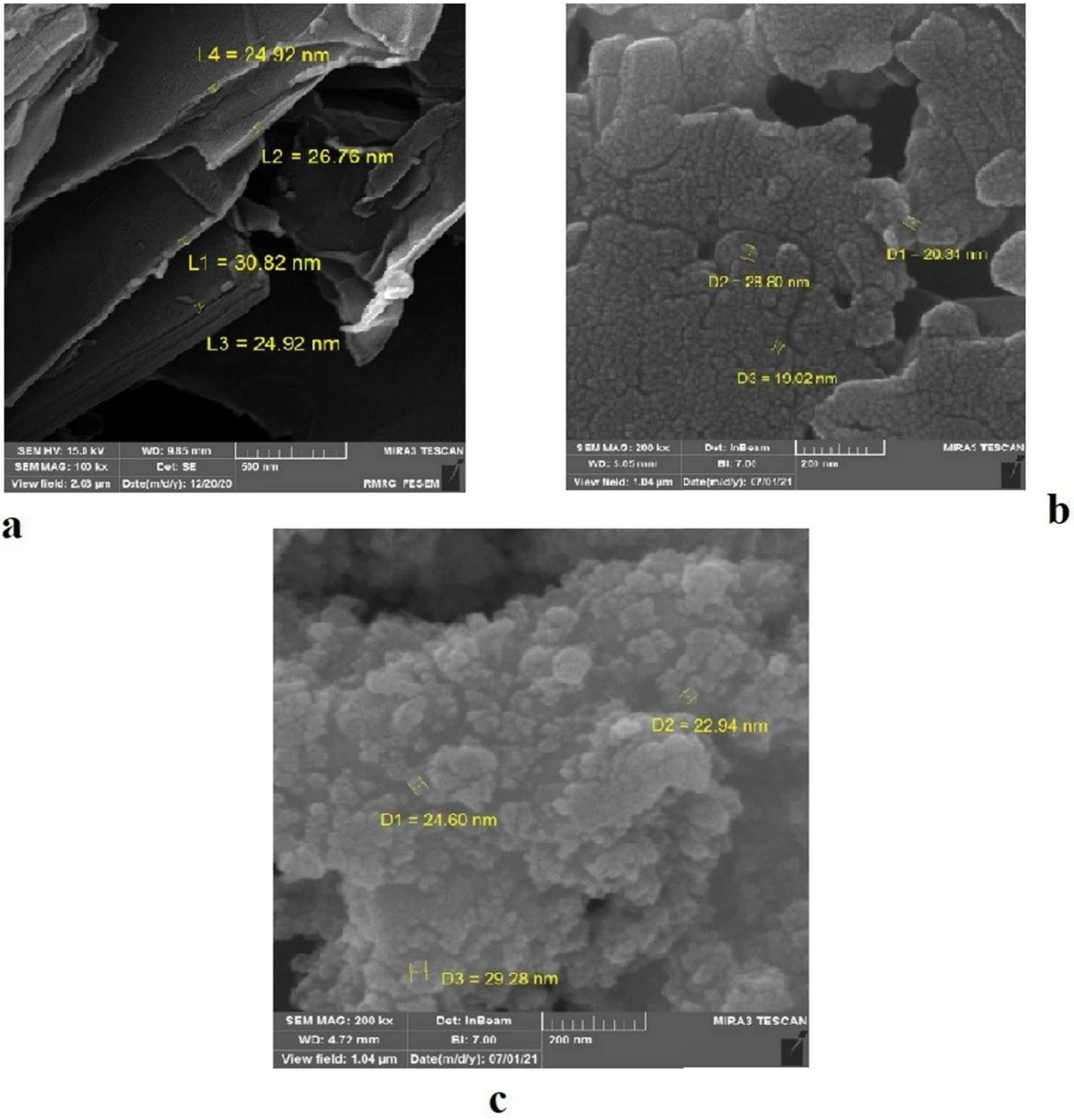

Fig. 3. FE-SEM images of (a) GO, (b) Bi_2Te_3/GO and (c) Bi_2Te_3/GO@4-AA.

a positive charge at pH amounts higher than 5.4 at the area of the nanoadsorbent. Also, around pH 5.4, the numbers of negative and positive sites of the nanoadsorbent are equal. Accordingly, the pH_{PZC} for Bi_2Te_3/GO@4-AA was found to be about 5.4 (Fig. 5b).

The influence of contact time on the removal of NP by Bi_2Te_3/GO@4-AA was investigated in different periods of time. The removal efficiency of NP was increased very fast within 15 min, slightly after 15 min and the removal efficiency of NP was constant. This behavior is related to the accumulation of adsorbent particles and the overlap of their active sites. According to the results, the optimal contact time was observed at 15 min (Fig. 5c).

Fig. 5d displays removal efficiency at different concentrations (2–40 mg L^{-1}) for NP. As shown in Fig. 5d, the removal efficiency of NP was increased rapidly when concentration ranged from 2 to 20 mg L^{-1}. The removal efficiency decreased when the amount of initial concentration raised from 20 to 40 mg L^{-1}. The optimum concentration was determined at 20 mg L^{-1}.

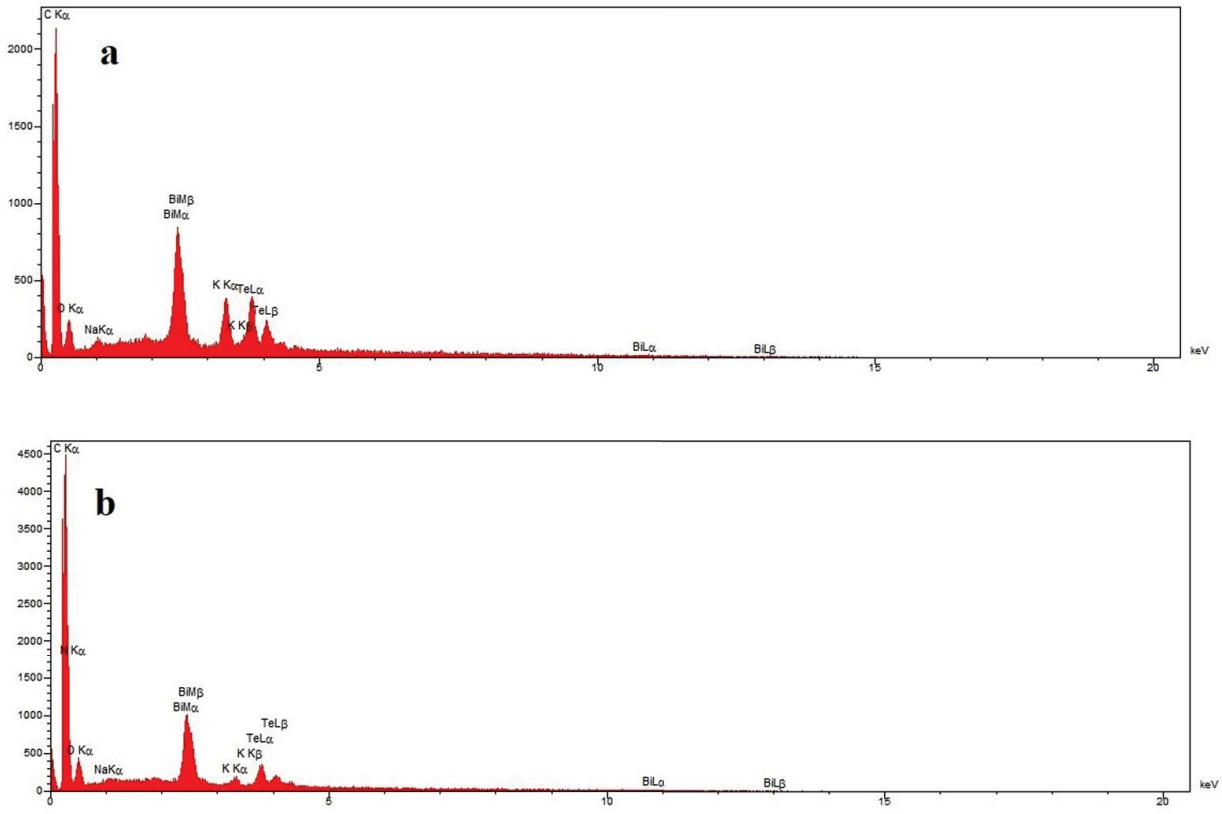

Fig. 4. EDX spectrum of (a) Bi_2Te_3/GO and (b) Bi_2Te_3/GO@4-AA.

The influence of different temperatures (20°C–40°C) on the NP removal was studies under optimized conditions (Fig. 5e). The removal efficiency decreased as the temperature increased from 20°C to 40°C. The highest removal efficiency was observed at 30°C. Accordingly, temperature no obvious effects on the adsorption.

3.3. Adsorption isotherms and kinetics

Table 1 indicated the parameters of Langmuir, Freundlich, Temkin, and Dubinin–Radushkevich isotherms for adsorption of NP onto the Bi_2Te_3/GO@4-AA at 25°C. As shown in Table 1, the correlation coefficient (R^2) values for Langmuir equation were higher than those of Langmuir, Freundlich and Temkin isotherm models. The Langmuir adsorption capacity (q_{max}) was 43.47 mg g^{-1} which represents that Bi_2Te_3/GO@4-AA shows important potential for the adsorption of NP. Also, the value of n, which is greater than 1, suggested that the adsorption of NP onto Bi_2Te_3/GO@4-AA was a favorable adsorption. Moreover, the adsorption intensity (R_L) was 0.106 shown that the adsorption process is favorable. Also, if $n > 1$, showing the physical adsorption of NP on the Bi_2Te_3/GO@4-AA.

In this paper, the three adsorption kinetic models (PFO, PSO and IPD) were used to further analyze the sorption mechanism of NP. The kinetic parameters for the PFO, PSO and IPD models were calculated from the linear plots of ln ($q_e - q_t$) vs. t, (t/q_e) vs. t, and q_t vs. $t^{1/2}$, respectively. The comparison of kinetic parameters were summarized in Table 2. From data in Table 2, the adsorption kinetics of NP were described better by PSO kinetic model compared to PFO and IPD. Moreover, the theoretical $q_{e,cal}$ values obtained from PSO model agreed more closely with the experimental values ($q_{e,exp}$).

3.4. Reusability of Bi_2Te_3/GO@4-AA

Reusability is effective to recover the adsorbed NP and for the reuse of the Bi_2Te_3/GO@4-AA. The reusability of Bi_2Te_3/GO@4-AA was examined at the concentration of 20 mg L^{-1} for each of NPs. To study the reusability of the Bi_2Te_3/GO@4-AA, ten consecutive adsorption–desorption cycles were carried out using methanol as a regenerating eluent. The adsorption–desorption cycles of Bi_2Te_3/GO@4-AA are shown in Fig. 6. As can be seen in Fig. 6, the removal efficiency of Bi_2Te_3/GO@4-AA for NP was decreased about 10% after regeneration at 5th cycle of reuse.

3.5. Application of Bi_2Te_3/GO@4-AA for real samples analysis

The Bi_2Te_3/GO@4-AA was applied to detect NP in various water samples and the results are listed in Table 3. To find relative removal and estimate accuracy of the procedure, spiking tests were performed. 0.98, 0.98, and 0.89 μg mL^{-1} of NP were found in Kan River, well water, and industrial wastewater samples, respectively. The industrial wastewater samples were analyzed without dilution. The recoveries range from 89.29% to 98.97% with RSDs < 5.6%

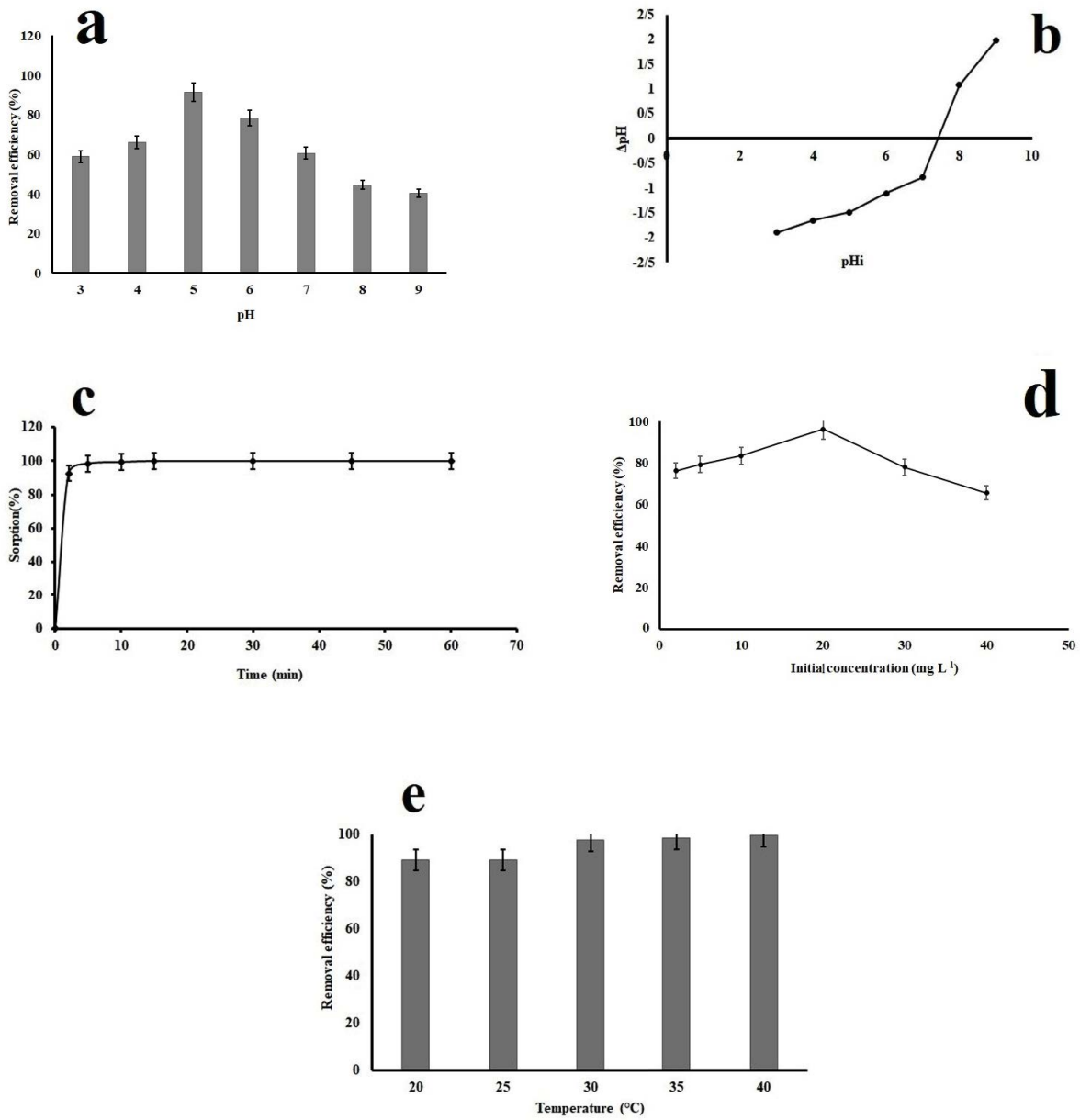

Fig. 5. Effect of (a) initial pH, (b) pH_{PZC}, (c) contact time, (d) initial concentration and (e) temperature on the removal of NP on Bi_2Te_3/GO@4-AA.

for the three water samples, which indicates that the procedure has good precision for the determination of NP in water samples. In comparison with removal efficiency of other reported adsorbents as listed in Table 4, the removal efficiency of NP by Bi_2Te_3/GO@4-AA are higher than most of the reported ones [35–38]. This data proposed that the suggested technique was accurate, suitable and selective for removal of NP from environmental samples.

3.6. Comparison with other procedures

The present technique based on high-performance liquid chromatography with fluorescence detector (HPLC-FD) was compared with some other reported techniques in terms of RSD and removal efficiency (Table 5). The HPLC-FD technique has the advantages of good removal, and satisfactory repeatability. The HPLC-FD technique that was utilized for the detection of NP is a well-known, robust, and comparatively inexpensive. Also, the synthesis of Bi_2Te_3/GO@4-AA is simple and doesn't require special method.

4. Conclusions

In summary, Bi_2Te_3/GO@4-AA nanoadsorbent was synthesized and evaluated for HPLC-FD of NP from water and industrial wastewater samples. The FTIR spectrum, SEM/EDX images, TGA curves, and XRD patterns indicated that

NP has been synthesized successfully. Also, the effect of different operational conditions like pH, initial concentration of NP, contact time, and temperature were evaluated. Batch tests proposed that Langmuir isotherm and pseudo-*second-order are well fitted to describe the isotherm and kinetic of adsorption, respectively. Also, the nanoadsorbent could be regenerated and recovered at optimum condition. The Bi_2Te_3/GO@4-AA is compared with other adsorbents and concluded that it is better than other adsorbents reported in previous literature. The prepared Bi_2Te_3/GO@4-AA nanoadsorbent was confirmed to possess good reusability, excellent adsorption efficiency, good adsorption capacity, and high removal for effective removal NP from aqueous media.

Table 1
Langmuir, Freundlich, Temkin and Dubinin–Radushkevich isotherm parameters for removal of NP onto the Bi_2Te_3/GO@4-AA

Model	Parameter	Value
Langmuir	q_{max} (mg g^{-1})	43.478
	K_L (L mg^{-1})	0.083
	R_L	0.106
	R^2	0.9927
Freundlich	n	1.206
	K_f (mg g^{-1})(L mg^{-1})$^{1/n}$	3.198
	R^2	0.8406
Temkin	A (L mg^{-1})	2.394
	B	5.583
	R^2	0.9436
Dubinin–Radushkevich	K_{DR} (mol^2 kJ^{-2})	0.000001
	q_s (mg g^{-1})	18.234
	R^2	0.9664

Table 2
PFO, PSO, and IPD kinetic parameters for removal of NP onto the Bi_2Te_3/GO@4-AA

Model	Parameter	Value
PFO	q_e (mg g^{-1})	1.454
	k_1 (min^{-1})	0.307
	R^2	0.953
PSO	q_e (mg g^{-1})	13.679
	k_2 (g mg^{-1} min^{-1})	0.809
	R^2	1
IPD	k_p (g mg^{-1} min$^{-0.5}$)	0.526
	C_i (mg g^{-1})	12.021
	R^2	0.8266

Acknowledgment

The authors would like to acknowledge Islamic Azad University (Science and Research Branch) for financial support of this project.

Table 4
Comparison of the removal efficiency of NP onto various adsorbents

Adsorbent	Removal (%)	References
Pectin-Fe_3O_4	62	[35]
BT-Fe_3O_4	73.3	[36]
Fe_3O_4/AC	73.3	[37]
PAMAM-MNP	63–70	[38]
Bi_2Te_3/GO@4-AA	89–98.98	This work

Table 5
Comparison of present technique with reported techniques for the detection of NP

Analytical technique	RSD (%)	Removal (%)	References
HPLC-VWD	2.12	96.0–96.5	[5]
HPLC-PDA	9.3	80.3–93.5	[39]
HPLC-UV	2.5	93.8–101.1	[7]
HPLC	2.5	93.4–96.2	[40]
HPLC-FD	<5.6	89.2–98.2	This study

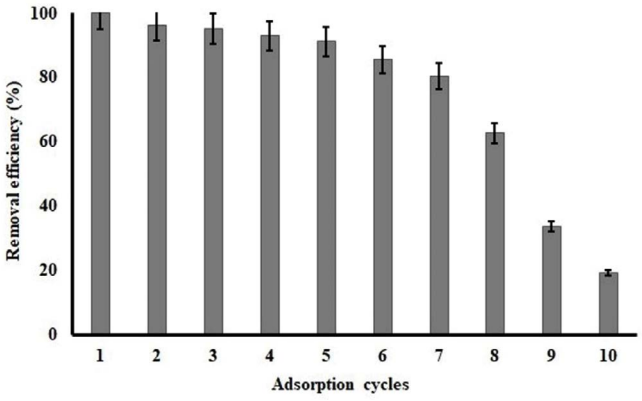

Fig. 6. Reusability of Bi_2Te_3/GO@4-AA for NP removal.

Table 3
Removal of NP in various environmental water samples (HPLC-FD)

Sample	Added (μg mL^{-1})	Found (μg mL^{-1})[a]	RSD (%)	Removal (%)
Kan River	1.00	0.98	5.58	98.29
Well water	1.00	0.98	1.93	98.97
Industrial wastewater	1.00	0.89	4.24	89.29

[a]For three experiments.

Symbols

q_e	—	Sorption capacity
C_e	—	Equilibrium concentration
C_0	—	Initial concentration
V	—	Volume of solution
M	—	Amount of nanoadsorbent
K_L	—	Langmuir constant
q_{max}	—	Maximum adsorption capacity
$1/n$	—	Intensity of adsorption
K_f	—	Freundlich constant
b	—	Heat of NP sorption
R	—	Universal gas constant
A	—	Temkin constant
T	—	Temperature
K_{DR}	—	Dubinin–Radushkevich constant
R^2	—	Correlation coefficient
ε	—	Polanyi potential
R_L	—	Separation factor
q_e	—	Adsorption amount of NP at equilibrium
q_t	—	Adsorption amount of NP at time
k_p	—	IPD rate constant
C_i	—	Intercept
k_1	—	PFO rate constant
k_2	—	PSO rate constant
t	—	Time

References

[1] S. Cen, Y. Chen, J. Tan, Y. Zhong, X. Luo, X. Pan, H. Wang, R. He, The fabrication of a highly ordered molecularly imprinted mesoporous silica for solid-phase extraction of nonylphenol in textile samples, Microchem. J., 164 (2021) 105954, doi: 10.1016/j.microc.2021.105954.

[2] A.R. Rahmani, M. Salari, A. Shabanloo, N. Shabanloo, S. Bajalan, Y. Vaziri, Sono-catalytic activation of persulfate by nZVI-reduced graphene oxide for degradation of nonylphenol in aqueous solution: process optimization, synergistic effect and degradation pathway, J. Environ. Chem. Eng., 8 (2020) 104202, doi: 10.1016/j.jece.2020.104202.

[3] L. Zheng, C. Zhang, J. Maa, S. Hong, Y. She, A.M. Abd EI-Aty, Y. He, H. Yu, H. Liu, J. Wang, Fabrication of a highly sensitive electrochemical sensor based on electropolymerized molecularly imprinted polymer hybrid nanocomposites for the determination of 4-nonylphenol in packaged milk samples, Anal. Biochem., 559 (2018) 44–50.

[4] B. Ba Mohammed, K. Yamni, N. Tijani, A.A. Alrashdi, H. Zouihri, Y. Dehmani, I.-M. Chung, S.-H. Kim, H. Lgaz, Adsorptive removal of phenol using faujasite-type Y zeolite: adsorption isotherms, kinetics and grand canonical Monte Carlo simulation studies, J. Mol. Liq., 296 (2019) 111997, doi: 10.1016/j.molliq.2019.111997.

[5] Q. Zhou, M. Lei, J. Li, K. Zhao, Y. Liu, Sensitive determination of bisphenol A, 4-nonylphenol and 4-octylphenol by magnetic solid phase extraction with Fe@MgAl-LDH magnetic nanoparticles from environmental water samples, Sep. Purif. Technol., 182 (2017) 78–86.

[6] G.G. Haciosmanoglu, Z. Yücesoy-Ozkan, Z. Semra Can, S. Genc, E. Soyer, E. Pehlivanoglu-Mantas, E. Erdim, Removal of nonylphenol and octylphenol from aqueous solutions by a novel nano-composite (ZVI/fullerene), Proceedings, 2 (2018) 654, doi: 10.3390/proceedings2110654.

[7] N. Al Rashed, K. Guenther, Determination of endocrine-disrupting nonylphenols and nonylphenol carboxylates by high-performance liquid chromatography-tandem mass spectrometry: levels in German food after restriction, Anal. Lett., 55 (2022) 634–647.

[8] S. Shariati, K. Yekeh Falah, A. Saleh, S. Molaei, Extraction and preconcentration of Bisphenol A and 4-Nonylphenol in aqueous solutions using microfunnel supported liquid-phase microextraction prior to high performance liquid chromatography, J. Iran. Chem. Soc., 18 (2021) 887–892.

[9] S. Erarpat, S. Bodur, D.S. Chormey, E. Öz, S. Bakırdere, Sensitive determination of 4-n-nonylphenol in domestic wastewater and liquid detergent by binary solvent microextraction (BSME) and gas chromatography–mass spectrometry (GC-MS) with matrix matching calibration, Anal. Lett., 55 (2022) 1080–1092.

[10] F.-F. Wu, Y. Zhu, X.-Y. Zhao, L.-Q. Qian, Y.-L. Wei, X.-J. Ma, M.-L. Ye, H.-R. Cui, Preparation of sheet-like covalent organic frameworks and their application for efficient preconcentration of 4-(tert-octyl)-phenol and 4-nonylphenol in textiles, J. Chromatogr. A, 1635 (2021) 461765, doi: 10.1016/j.chroma.2020.461765.

[11] B. Ringbeck, D. Bury, H. Hayen, T. Weiss, T. Brüning, H.M. Koch, Determination of specific urinary nonylphenol metabolites by online-SPE-LC-MS/MS as novel human exposure biomarkers, J. Chromatogr. B, 1177 (2021) 122794, doi: 10.1016/j.jchromb.2021.122794.

[12] L. Lou, Q. Huang, Y. Lou, J. Lu, B. Hu, Q. Lin, Adsorption and degradation in the removal of nonylphenol from water by cells immobilized on biochar, Chemosphere, 228 (2019) 676–684.

[13] Å. Stenholm, M. Hedeland, T. Arvidsson, C.E. Pettersson, Removal of nonylphenol polyethoxylates by adsorption on polyurethane foam and biodegradation using immobilized *Trametes versicolor*, Sci. Total Environ., 724 (2020) 138159, doi: 10.1016/j.scitotenv.2020.138159.

[14] Z. Wang, X. Wang, X. Li, H. Zhang, J. Wei, Y. Zhou, Effect of structure matching in the adsorption process: the preparation of alkylbenzene-functionalized polypropylene nonwoven using surface modification for adsorbing nonylphenol, React. Funct. Polym., 163 (2021) 104874, doi: 10.1016/j.reactfunctpolym.2021.104874.

[15] Y. Li, S. Wang, H. Li, G. Kang, Y. Sun, H. Yu, Y. Jin, Y. Cao, Preparation of highly selective nanofiltration membranes by moderately increasing pore size and optimizing microstructure of polyamide layer, J. Membr. Sci., 643 (2022) 120056, doi: 10.1016/j.memsci.2021.120056.

[16] C.-Y. Chen, M.-L. Tsai, Tris(imidazolyl) dicopper(I) complex and its reactivity to exert the catalytic oxidation of sterically hindered phenol substrates *via* a $[Cu_2O]^{2+}$ core, Dalton Trans., 51 (2022) 2428–2443.

[17] L. Yang, R. Yi, C. Yi, H. Yu, J. Zhang, M.I. Nawaz, Degradation of the nonylphenol aqueous solution by strong ionization discharge: evaluation of degradation mechanism and the water toxicity of zebrafish, Water Sci. Technol., 86 (2022) 227–243.

[18] G.T. Tee, X.Y. Gok, W.F. Yong, Adsorption of pollutants in wastewater via biosorbents, nanoparticles and magnetic biosorbents: a review, Environ. Res., 212 (2022) 113248, doi: 10.1016/j.envres.2022.113248.

[19] F. Einollahi Peer, N. Bahramifar, H. Younesi, Removal of Cd(II), Pb(II) and Cu(II) ions from aqueous solution by polyamidoamine dendrimer grafted magnetic graphene oxide nanosheets, J. Taiwan Inst. Chem. Eng., 87 (2018) 225–240.

[20] X. Wang, Y. Guo, Z. Jia, H. Ma, C. Liu, Z. Liu, Q. Shi, B. Ren, L. Li, X. Zhang, Y. Hu, Fabrication of graphene oxide/polydopamine adsorptive membrane by stepwise in-situ growth for removal of rhodamine B from water, Desalination., 516 (2021) 115220, doi: 10.1016/j.desal.2021.115220.

[21] Q. Lian, F. Islam, Z.U. Ahmad, X. Lei, D. Depan, M. Zappi, D.D. Gang, W. Holmes, H. Yan, Enhanced adsorption of resorcinol onto phosphate functionalized graphene oxide synthesized via Arbuzov reaction: a proposed mechanism of hydrogen bonding and π-π interactions, Chemosphere, 280 (2021) 130730, doi: 10.1016/j.chemosphere.2021.130730.

[22] C. Kulsi, M. Mitra, K. Kargupta, D. Banerjee, Thermoelectric properties of nanostructured bismuth telluride (Bi_2Te_3) with annealing time and its composite with reduced graphene oxide (RGO), J. Mater. Sci.: Mater. Electron., 30 (2019) 1850–1860.

[23] B.B. Liang, Z.J. Song, M.H. Wang, L.J. Wang, W. Jiang, Fabrication and thermoelectric properties of graphene/composite materials, J. Nanomater., 2013 (2013) 1–5.
[24] K. Agarwal, V. Kaushik, D. Varandani, A. Dhar, B.R. Mehta, Nanoscale thermoelectric properties of Bi_2Te_3-graphene nanocomposites: conducting atomic force, scanning thermal and kelvin probe microscopy studies, J. Alloys Compd., 681 (2016) 394–401.
[25] S. Kumar, S. Singh, P.K. Dhawan, R.R. Yadav, N. Khare, Effect of graphene nanofillers on the enhanced thermoelectric properties of Bi_2Te_3 nanosheets: elucidating the role of interface in de-coupling the electrical and thermal characteristics, Nanotechnology, 29 (2018) 135703.
[26] J. Yun, I. Echols, P. Flouda, Y. Chen, S. Wang, X. Zhao, D. Holta, M. Radovic, M.J. Green, M. Naraghi, J.L. Lutkenhaus, Layer-by-layer assembly of reduced graphene oxide and MXene nanosheets for wire-shaped flexible supercapacitors, ACS Appl. Mater. Interfaces, 13 (2021) 14068–14076.
[27] X. Jiang, W. Pan, Z. Xiong, Y. Zhang, L. Zhao, Facile synthesis of layer-by-layer decorated graphene oxide based magnetic nanocomposites for β-agonists/dyes adsorption removal and bacterial inactivation in wastewater, J. Alloys Compd., 870 (2021) 159414, doi: 10.1016/j.jallcom.2021.159414.
[28] I. Langmuir, The adsorption of gases on plane surfaces of glass, mica and platinum, J. Am. Chem. Soc., 40 (1918) 1361–1403.
[29] H.M.F. Freundlich, Über die Adsorption in Lösungen, Z. Phys. Chem. (Leipzig), 57 (1906) 385–470.
[30] M.I. Temkin, Adsorption equilibrium and kinetics of processes on heterogeneous surfaces and at interaction between adsorbed molecules, Zh. Fiz. Khim. (Russ. J. Phys. Chem.), 15 (1941) 296–332.
[31] M.M. Dubinin, The potential theory of adsorption of gases and vapors for adsorbents with energetically non-uniform surface, Chem. Rev., 60 (1960) 235–266.
[32] E. Daneshmoghanlou, M. Miralinaghi, E. Moniri, S.K. Kazem Sadjady, Fabrication of a pH-responsive magnetic nanocarrier based on carboxymethyl cellulose-aminated graphene oxide for loading and in-vitro release of curcumin, J. Polym. Environ., 30 (2022) 3718–3736.
[33] M. Pour Shaban, E. Moniri, R. Safaeijavan, H. Ahmad Panahi, Kinetics, isotherm and adsorption mechanism studies of letrozole loaded modified and biosynthesized silver nanoparticles as a drug delivery system: comparison of nonlinear and linear analysis, Korean Chem. Eng. Res., 59 (2021) 493–502.
[34] A. Homayonfard, M. Miralinaghi, R. Haji Seyed Mohammad Shirazi, E. Moniri, Efficient removal of cadmium(II) ions from aqueous solution by $CoFe_2O_4$/chitosan and $NiFe_2O_4$/chitosan composites as adsorbents, Water Sci. Technol., 78 (2018) 2297–2307.
[35] Y. Uysal, P. Belibağlı, Removal of nonylphenol ethoxylates from water by using pectin coated nano magnetite composite (Pectin-Fe_3O_4), Pamukkale Univ. J. Eng. Sci., 25 (2019) 929–937.
[36] P. Belibağli, Y. Uysal, Green synthesis of BT-Fe_3O_4 nanocomposite using *Camellia sinensis* leaves extract: characterization, NPEO adsorption experiments, isotherms, and kinetics, Sigma J. Eng. Nat. Sci., 40 (2022) 132–143.
[37] X. Li, S. Chen, L. Li, X. Quan, H. Zhao, Electrochemically enhanced adsorption of nonylphenol on carbon nanotubes: kinetics and isotherms study, J. Colloid Interface Sci., 415 (2014) 159–164.
[38] V. Khatibikamal, H. Ahmad Panahi, A. Torabian, M. Baghdadi, Optimized poly(amidoamine) coated magnetic nanoparticles as adsorbent for the removal of nonylphenol from water, Microchem. J., 145 (2019) 508–516.
[39] A. Sun, Q. Xu, X. Yu, Determination of bisphenol A and 4-nonylphenol in water using ionic liquid dispersive liquid phase microextraction, Pol. J. Environ. Stud., 22 (2013) 899–907.
[40] Q. Zhou, Y. Yuan, Y. Wu, Y. Liu, Sensitive determination of typical phenols in environmental water samples by magnetic solid-phase extraction with polyaniline@SiO_2@Fe as the adsorbents before HPLC, J. Sep. Sci., 40 (2017) 4032–4040.